ACS OMEGA

http://pubs.acs.org/journal/acsodf

Mini-Review

Simultaneous Electrical and Mechanical Characterization of Single-Molecule Junctions Using AFM-BJ Technique

Yixuan Zhu, Zhibing Tan,* and Wenjing Hong*

Cite This: *ACS Omega* 2021, 6, 30873−30888

Read Online

ACCESS | Metrics & More | Article Recommendations

ABSTRACT: The fabrication and characterization of single-molecule junctions provide a unique platform to study the physical phenomena of a single molecule, and the electrical characterization enables us to understand the electrical transport properties of a single molecule and guide the fabrication of molecular electronic devices. However, the electrical characterization of single-molecule junctions is sometimes insufficient to extract the structural information on single-molecule junctions, and an alternate method to address this problem is to characterize the mechanical properties of single-molecule junctions. Simultaneous measurement of mechanical and electrical properties can provide complementary information on single molecules to analyze the correlations of their electrical and mechanical properties in the evolution of single-molecule junctions. In this mini-review, we summarize the progress on the simultaneous characterizations of mechanical and electrical properties for single-molecule junctions, and discuss the challenges and perspectives of this research area.

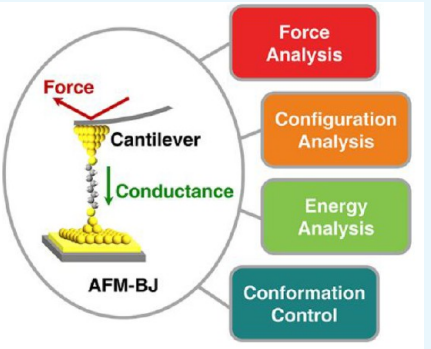

1. INTRODUCTION

Inspired by the idea that molecules could serve as functional building blocks in electronic devices,[1] scientists all over the world have been exploring the electrical properties of single-molecule junctions experimentally and theoretically during the past decades.[2] To characterize the charge transport phenomena of a single molecule, a molecule is usually captured by two microelectrodes to form a single-molecule junction. Most of the studies on molecular electronics are focused on the measurement of conductance of the single-molecule junctions. However, the structural information about single-molecule junctions sometimes cannot be obtained from the electrical characterization. Simultaneous measurement of mechanical and electrical properties can provide additional information to improve the understanding of molecular configuration in the single-molecule junctions.[3]

On the basis of atomic force microscope (AFM), the conducting probe atomic force microscope break junctions (cpAFM-BJ or AFM-BJ) technique[4] uses a conductive probe with a cantilever, and combines the inherent laser system of AFM with the current measurement circuit, allowing the force and conductance signal during break junction process to be measured simultaneously. At the end of the 20th century, Rubio et al. reported the simultaneous measurement of force and conductance of the Au atom junction by AFM for the first time.[5] Xu et al. combined the break junctions technique with the force measurement of AFM, proving that the AFM technique is feasible to extend from metal atom-scaled contacts to the measurement of mechanical and electrical characterization of single-molecule junctions.[4a] Based on simultaneously measured forces and electrical signals, the rupture force of single-molecule junctions can be obtained, which can be used as a criterion for the existence of single-molecule junctions. With the improvement of testing techniques and the development of analytical methods, progress has been made in deciphering the structure−function correlations of single-molecule junctions; for example, force analysis provides a simple characterization of the molecule−electrode connecting form,[4b,6] and configuration analysis plots a more detailed view which refers to the dynamic evolution of single-molecule junctions.[3a−c] Energy analysis quantifies the current-induced local heat and the binding energy of molecule−electrode,[7] and by quantitatively regulating the tip−sample force, molecular conformation control can also be realized.[8]

In this mini-review, we summarize the study progress of measuring single-molecule junctions using the AFM-BJ technique. The application of force analysis in break junctions is introduced first, and the configuration analysis of single-molecule junctions, which involves diverse analytical methods, is highlighted. Energy analysis of the molecule−electrode interface involving the establishment of the theoretical model is also introduced. The studies of molecular conformation controlling

Received: August 31, 2021
Accepted: October 29, 2021
Published: November 12, 2021

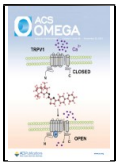

https://doi.org/10.1021/acsomega.1c04785
ACS Omega 2021, 6, 30873−30888

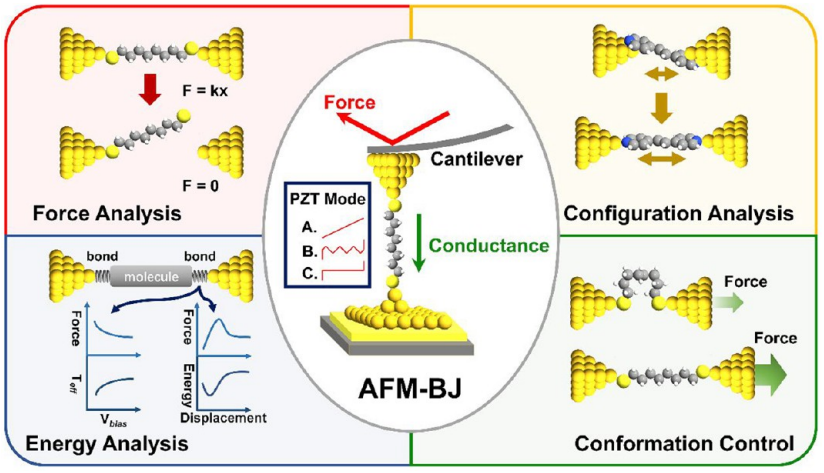

Figure 1. Schematic diagram of AFM-BJ technique and the research directions based on it.

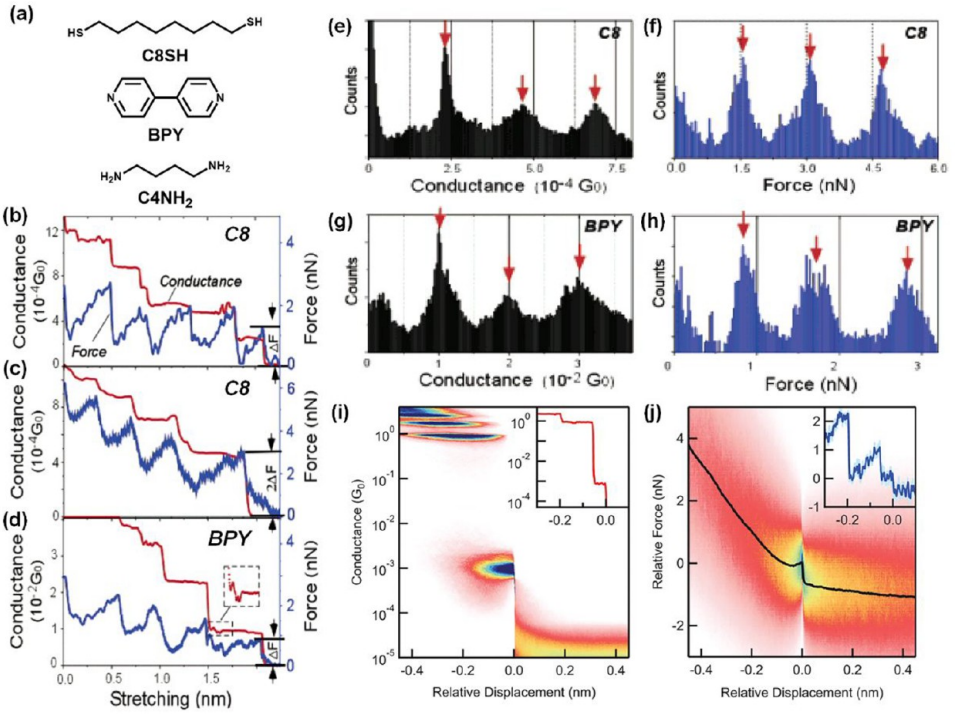

Figure 2. (a) Chemical structures of C8SH, BPY, and C4NH$_2$. Representative simultaneously measured force and conductance traces of C8SH (b,c) and BPY (d). 1D conductance and force histogram of C8SH (d,e) and BPY (f,g). 2D conductance and force histogram of 1,4-butanediamine (h,i). Some of the subgraphs are reprinted in part with permission from ref 4a. Copyright 2003 American Chemical Society; from ref 4b. Copyright 2011 American Chemical Society.

using a modified AFM-BJ technique are presented, and the challenges and perspectives for AFM-BJ technology are discussed in the last part of this mini-review.

2. RESEARCH PROGRESS OF SIMULTANEOUS ELECTRICAL AND MECHANICAL CHARACTERIZATION OF SINGLE-MOLECULE JUNCTIONS

Since 2003, Xu et al. used the AFM-BJ technique to measure the mechanical and electrical properties of single-molecule junctions,[4a] and the method has gradually become a tool to characterize the structure of single-molecule junctions. This pioneering study was based on the traditional break junction technology, and the obtained sawtoothed force traces contain intact mechanical information during the break junction process.

As shown in Figure 1, with the continuous innovation of measurement techniques and data analysis methods, the application of AFM-BJ has expanded to various research systems. The primal study of AFM-BJ technique is the force analysis of single-molecule junctions, providing a simple characterization of the molecule−electrode connecting form, and proving that the measured conductance originated from single-molecule junctions. Based on force histogram analysis, a series of rupture forces of single-molecule junctions were measured.[4b,6] Subsequently, the research extended from the analysis of single-molecule junctions to more complex supramolecular systems, and the distinctive weak rupture force makes

https://doi.org/10.1021/acsomega.1c04785
ACS Omega 2021, 6, 30873−30888

it suitable for force analysis.[9] Subsequent research focused on the relationship between electrical and mechanical properties of single-molecule junctions. The correlation analysis of conductance and force can effectively reveal the configuration change of break junctions,[3a−c] and the involvement of the controllable mechanical modulation technique promotes the further study of the dynamic process of single-molecule junctions.[10] It can hold the single-molecule junctions for a moment or even add a regular mechanical oscillation, and the dynamic variation of contact configuration of the molecule−electrode interface during oscillation can be studied.[11] The close relationship between force and energy also makes it possible to study the heat and energy at the molecule−electrode interface using AFM-BJ, and the difficulty lies in the establishment of the theoretical model. The effect of thermal fluctuations on the rupture force causes the temperature change between the molecule−electrode interfaces to become measurable.[7a] On the other hand, the integral of the force traces corresponds to the bond energy. The characteristics of potential energy surface during the rupture of single-molecule junctions were obtained by fitting a hybrid model, which made it possible to measure bond energy experimentally.[7b] Furthermore, assisted by tactile-feedback controlled conductive AFM, the relationship between molecular conformation and conductance can even be studied by controlling the tip−sample force.[8]

2.1. Force Analysis of Atomic-Scaled Junctions. *Single-Molecule Junctions.* The force and conductance traces obtained synchronously are shown in Figure 2b−d, while the force traces feature with the sawtooth. The rupture point of the single-molecule junctions can be quickly found through the position of the molecular conductance plateau in the conductance traces, and the 1D force histogram can be obtained through statistical analysis of the force difference before and after the rupture of the single-molecule junction (Figure 2f and h). The corresponding 1D conductance histogram can also be obtained simultaneously (Figure 2e and g). Xu et al. measured the rupture force of Au point contacts, C8SH and BPY junctions (Figure 2a) based on the 1D force histogram.[4a] Because the values of forces before and after the rupture should be calculated for every force curve, this method introduces considerable uncertainty, especially for junctions with relatively small rupture force. To further improve the data accuracy, Frei et al. developed the 2D force histogram.[4b] The rupture point of single-molecule junctions found through conductance traces was set as the zero point of the displacement axis, and the maximum force value at the rupture point of junctions was shifted to the origin of coordinates by subtracting an offset from the entire force trace. All the force curves are overlaid statistically. By fitting the vertical sections at every displacement bin through Gaussian distribution, a statistically averaged force trace was obtained. Figure 2i,j shows the 2D conductance and force histograms of $C4NH_2$. The differences in rupture force of the Au−N bond using amino and pyridyl as anchoring groups were compared through the method. Ahn et al. also measured the breaking force of the carboxyl group as an anchor group using a 2D force histogram.[6] A rupture force of 0.6 ± 0.1 nN suggests that COO^--Au has excellent mechanical stability comparable to the Au-SMe bond.

For the molecule with destructive quantum interference, it is difficult to measure the conductance because of the poor conductivity, but rupture force may provide more direct evidence for the existence of the single-molecule junctions. Aradhya et al. analyzed contact mechanics of stilbene derivatives (Figure 3a)[12] and realized the first study of mechanical

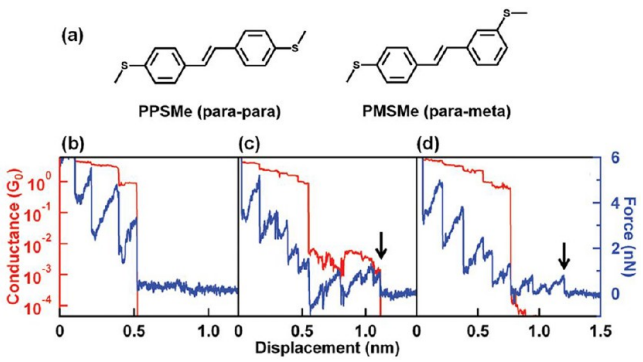

Figure 3. (a) Chemical structures of PPSMe and PMSMe. Representative traces of simultaneously measured force and conductance for (b) Au−Au junctions, (c) Au−PPSMe−Au, and (d) Au−PMSMe−Au single-molecule junctions. Adapted from ref 12. Copyright 2012 American Chemical Society.

properties of single-molecule junctions with destructive quantum interference effect. The conductance curve of PMSMe (Figure 3d) is the same as that of the Au−Au junction (Figure 3b), with no obvious conductance platform observed because of destructive quantum interference. However, force analysis finds that PMSMe has the same value of rupture force as PPSMe (Figure 3c), which proves the existence of PMSMe junctions. These results demonstrate that quantum interference is an inherent nature generated by molecular structure.

Single-Supramolecule Junctions. The study of electrical transport through intermolecular interaction is much more complicated than through a single molecule.[13] The characteristic weak rupture force can provide evidence that the conductance is derived from a single-supramolecule junction. In 2015, Yoshida et al. performed the electronic and mechanical characteristics of stacked dimer molecule junctions using tolane-type molecules, which can form $\pi-\pi$ stacking dimers.[14] Tolane-type molecules always have two distinct conductance platforms. The rupture forces of single-molecule junctions were characterized as a function of their conductance before breaking. The rupture force of the high conductance peak was much larger than that of the low conductance peak, which means that the former was originated from monomer molecule junctions and the latter to $\pi-\pi$ stacking dimers.

Single-molecule junctions formed by intermolecular interactions are characterized not only by weak rupture forces. With the help of diverse data analysis methods, Magyarkuti et al. further explored single-supramolecule junctions.[9] Similar to tolane-type molecules, molecules such as DAT (Figure 4a) and DAF (Figure 4b) have two distinct conductance plateaus, which may be caused by $\pi-\pi$ stacking (Figure 4c and d). The traditional 2D force histogram cannot compare the rupture force of two or more rupture events on a single trace, and then a new type of scaled 2D force histogram was introduced to analyze the data. The two rupture regions aligned along the horizontal axis, and the measured traces were overlaid. This method may lose displacement information, but force information is still intact. The rupture force can be determined by measuring the average force curve at the point where the single-molecule junctions rupture (Figure 4e and g). The weak rupture force of the low conductance plateau is obtained from the 2D force histogram and combined with conductance data and flicker noise power (PSD) analysis, and the authors concluded that the low conductance plateau comes from $\pi-\pi$ stacking dimers. Further

https://doi.org/10.1021/acsomega.1c04785
ACS Omega 2021, 6, 30873−30888

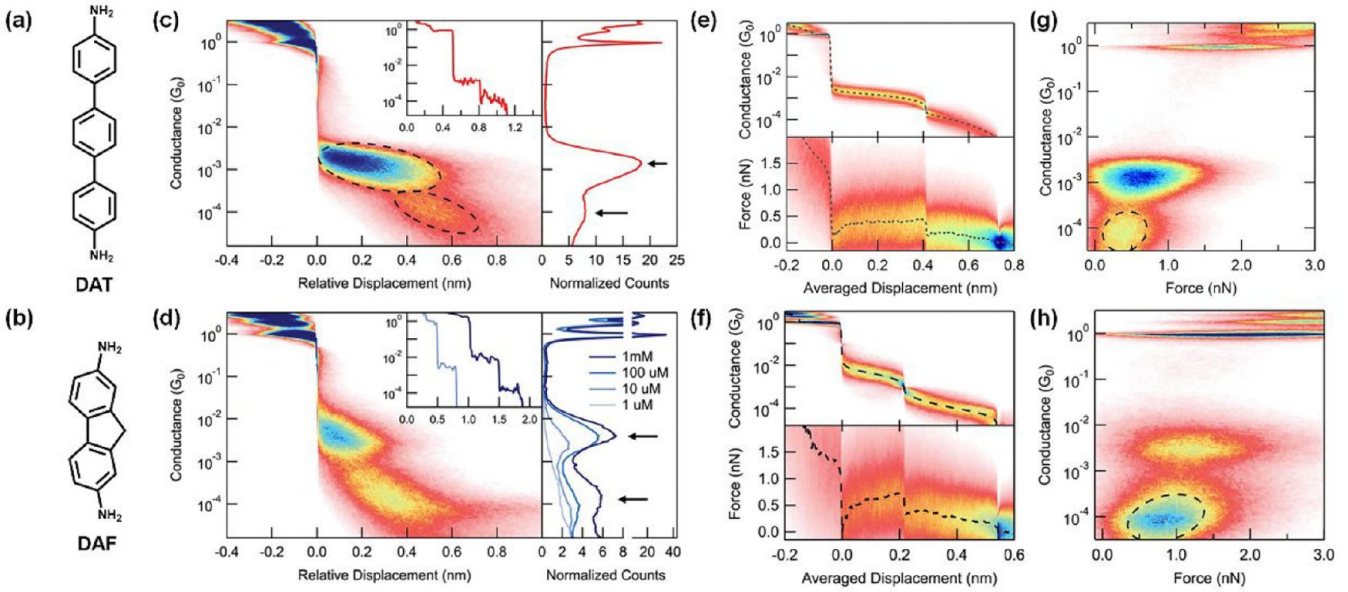

Figure 4. Structure of DAT (a) and DAF (b), and conductance histograms of DAT (c) and DAF (d). Scaled conductance (top) and force (bottom) histograms of DAT (e) and DAF (f). Conductance versus force histogram of DAT (g) and DAF (h). Adapted with permission from ref 9. Copyright 2018 the Royal Society of Chemistry.

study used the 2D conductance versus force histogram which was acquired by plotting every single trace of conductance data against force data and overlaying all the resulting traces. The tilted feature indicating conductance and force has a positive correlation which means the property of dimer junctions (Figure 4g and h, dashed line).

2.2. Configuration Analysis of Molecular Junctions. Unlike the force analysis which only focuses on the force events at the rupture point, contact configurations and structural rearrangement of the molecule−electrode interface involve a very complex dynamic process.[15] AFM-BJ can give more information about molecular junctions than single conductance measurements, and the dynamic process can be observed experimentally. The correlation analysis of conductance and force makes it easier to map the configurations of the molecule−electrode interface.

Using the AFM-BJ technique, Aradhya et al. characterized the force and conductance of BPY and BPE junctions (Figure 5a).[3c] Both molecules show a high conductance plateau around 10^{-3} G_0 (BPY_H and BPE_H) and a low one around 10^{-4} G_0 (BPY_L and BPE_L) (Figure 5b and c). It was found that the force traces go through several noticeable sawtooth changes, while the conductance traces remain unchanged (Figure 5d and e), which suggests that the high conductance plateau undergoes a rearrangement process. Further analysis of rupture force curves shows that the average rupture forces of both BPY_L and BPE_L are 0.8 nN, which is smaller than the Au−Au bond, while the rupture forces of BPY_H and BPE_H are 1.5 nN and 1.9 nN, respectively, which are not weaker than the Au−Au bond. The stiffness of BPY_H and BPE_H is also larger than that of the Au−Au bond. Combined with rupture force, stiffness, and rearrangement length analysis, the evolution process of the single-molecule junctions is deduced as illustrated in Figure 5f. The Au substrate may present undercoordinated sites which can support N−Au bonds, and adjacent larger Au uplift structures have van der Waals (vdW) interactions with the pyridine rings, which results in the high-conductance plateaus.

Combined with time series analysis (TSA) technology, the dynamic evolution process of single-molecule junctions can be analyzed in more detail. Cross-correlation is one of the time series analysis (TSA) techniques. Hamill et al. analyzed the evolution process of BPY single-molecule junctions through the force-conductance 2D cross-correlation histogram (FC-2DCCH).[16] As shown in Figure 6b, the sawtooth force traces can be converted into a step shape by removing the common slope associated with the constant retracement rate of the cantilever. Then 1D force histogram (Figure 6a) and 1D conductance histogram (Figure 6c) were obtained, and the peak values were 0.68 nN and 8.65×10^{-3} G_0, respectively. To eliminate the global trend, this study only focused on events within a short time scale around the plateau region of the peak value (8.65×10^{-3} G_0). Both of the average values of conductance and force for each trace were calculated, and then the average subtracted to offset each trace to zero. This ensured that the correlation analysis only considered the changes of force ΔF and conductance ΔG with respect to the plateau region, and the FC-2DCCH was subsequently obtained by cross-correlation calculations. Combining with the DFT simulation, the slight changes of the molecular structure during break junctions can be plotted. As shown in Figure 4f, the black circle (ΔF = 0.1 nN; $\Delta G = 6.0 \times 10^{-4}$ G_0) corresponds to the molecular torsion at the beginning of the break junctions. During the torsional relaxation, the distance between the π-orbital of the molecule and the s-orbital of Au gradually returns to the overlapped direction, resulting in a sudden change in force and conductance simultaneously. The black square ($\Delta F = -0.40$ nN; $\Delta G = 1.2 \times 10^{-4}$ G_0) corresponds to nitrogen atom slipping from the low spot of the Au electrode to the adjacent Au uplifted structures, which results in another sudden change. This area is similar to the change marked by the arrow in Figure 6e.

Molecules with thiol as an anchoring group tend to have multiple conductance plateaus, but the reason for this is unclear.[17] Early in 2006, Li et al. investigated the origin of this phenomenon using the AFM-BJ technique.[18] They found that C8SH had two conductance features (H and L in Figure 7c). It

https://doi.org/10.1021/acsomega.1c04785
ACS Omega 2021, 6, 30873−30888

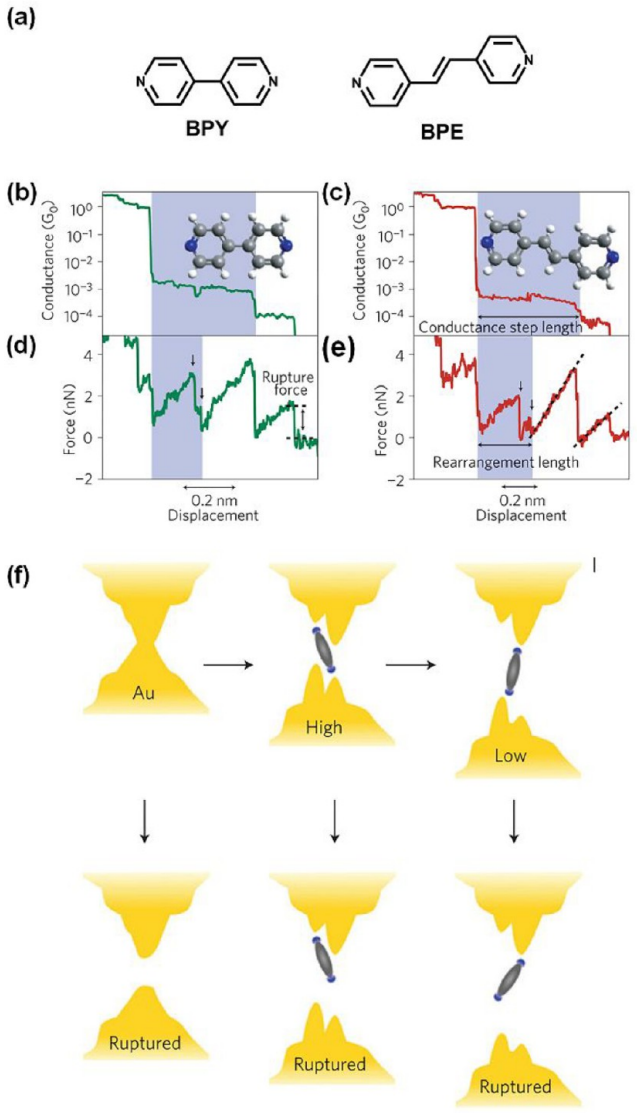

Figure 5. (a) Structure of BPYand BPE. Representative conductance (BPY (b) and BPE (c)) and force traces (BPY (d) and BPE (e)) during break junctions. (f) Schematic illustration of structural evolution pathways. Adapted with permission from ref 3c. Copyright 2012 Springer Nature.

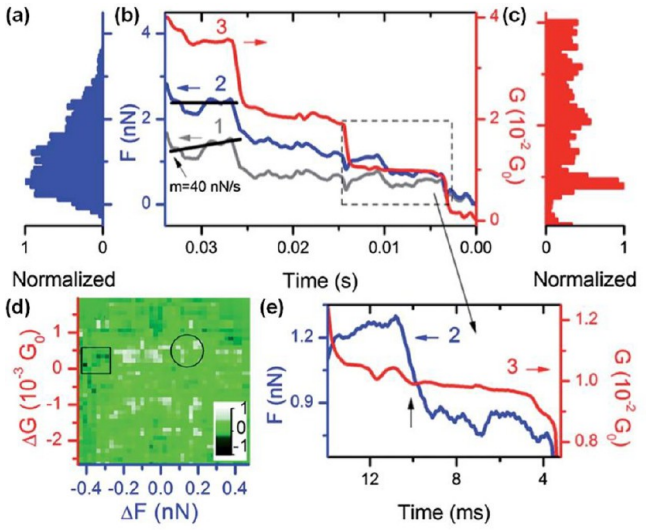

Figure 6. (a) 1D force histogram of BPY from constant-slope-adjusted force traces. (b) Representative force and conductance traces. (c) 1D conductance histogram of BPY. (d) Force-conductance 2D cross-correlation histogram of BPY. (e) Examples of the platform correlations of force and conductance. Adapted with permission from ref 16. Copyright 2014 the Royal Society of Chemistry.

was found that a conductance trace may raise an L step following an H step but the opposite never happens. The two conductance features had the same rupture force value of about 1.5 nN (Figure 7a and b), similar to the Au−Au bond. It was concluded that the H step corresponds to a molecule with one end sitting on a hollow site of the Au electrode while another is on a top site, or top-hollow geometry; the L step corresponds to a top−top geometry (Figure 7d). This explains why the L step can appear after an H step, but the opposite cannot occur. Although this conclusion explains the experimental phenomenon, this conclusion is in a sense speculative.

Thanks to the improvement of analytical methods, the study of the Au−S bond configuration can go a step further. Nef et al. studied the mechanical and electrical properties of C8SH and mC8SH by analyzing the 2D conductance versus force histogram.[19] Figure 8b shows the 2D histograms of C8SH (upper panel) and mC8SH (lower panel) and the corresponding 1D conductance and force histograms. The conductance histogram shows that the molecular conductance G_{mol} is $1.1 \times 10^{-5}G_0$. The force histogram of C8SH above the noise (open bars) does not show a significant peak instead of a shoulder around 1 nN (arrow), but it can be seen from the 2D histogram that there is a considerable force value above 0.8 G_{mol}. By subtracting the force below $0.8G_{mol}$, the force histogram shows a peak (solid bars) and the average rupture force above $0.8G_{mol}$ is 1.6 ± 0.4 nN. Furthermore, the average rupture force corresponding to the molecular conductance is analyzed and the value is 1.5 ± 0.4 nN, which is similar to that of the gold−gold junction. In contrast, the histograms of mC8SH do not show an obvious peak. This further confirms that the molecule junctions may undergo a rearrangement process before the junction breaks. The 2D conductance versus force histograms of C4SMe and C4SH were analyzed (Figure 9d).[3a] The histogram (Figure 9a top) shows that C4SMe has a well-defined conductance value, which means the structural rearrangements of C4SMe have less effect on conductance. However, C4SH shows an average of several force events for each trace which indicates that more rearrangement is performed during the break junction (Figure 9a bottom). As shown in Figure 9b, a 1D force histogram analysis of the force events within the dashed box in Figure 8a indicates that C4SH can form a donor−acceptor bond similar to C4SMe (Figure 9e). The maximal rupture/rearrangement force histogram per trace with conductance conforms to molecular characteristics showing that the most probable rupture force of C4SH is 1.2 nN, which is lower than that of the Au−Au bond (Figure 9c). This indicates that the rearrangement process does not need to rupture the single gold atom contacts. Combined with molecular dynamics simulation analysis, it is speculated that the molecular bond formed by the Au−S bond may result in a variety of adsorption configurations during break junctions, and the rupture may occur in both the Au−S bond and Au−Au bond. The terminal Au atom may be attached to one side of the electrode, analogous to hollow geometry (Figure 9f); an angle may be formed between the molecular backbone and the electrode (Figure 9g) or the Au

https://doi.org/10.1021/acsomega.1c04785
ACS Omega 2021, 6, 30873−30888

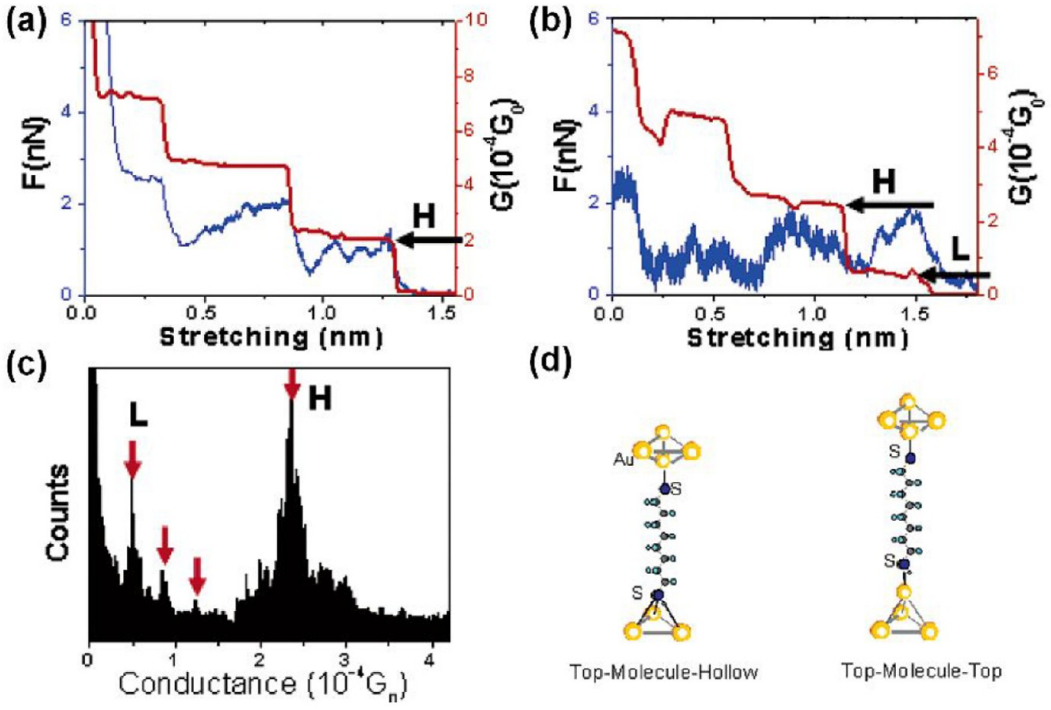

Figure 7. (a) Conductance and force traces which have only H steps. (b) Conductance and force traces have H steps followed by L steps. (c) 1D conductance histogram of C8SH. (d) Models of molecule−electrode contact geometries. Adapted from ref 18. Copyright from 2006 American Chemical Society.

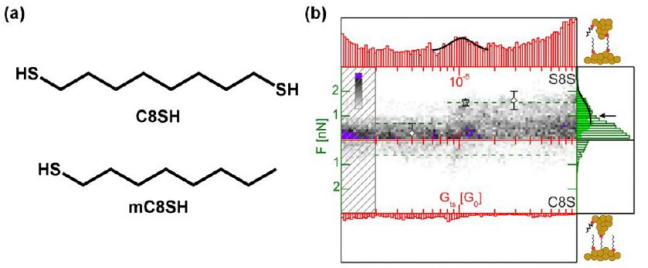

Figure 8. (a) Structure of C4SMe and C4SH. (b) 2D conductance versus force histogram; 1D force and 1D conductance histogram for C8SH (upper panel) and mC8SH (lower panel). Adapted from ref 19. Copyright from 2012 American Chemical Society.

atom coordination which is bond to S atom is different (Figure 9h). The strength of the Au−S bond and the flexibility of Au lead to rearrangement synergistically. However, the force and conductance signals are not assigned to the corresponding metal−molecule junction structure.

Zhou et al. developed a new technique called controllable mechanical modulation based on AFM-BJ.[10,11,20] The process of the break junction was modified: After the abrupt stretching of the tip over a short distance, the single-molecule junctions held for a moment, and then the conductance could be measured without the disturbance caused by retracting the tip, which is called the "stretching-holding" approach.[10a] This approach minimized the variations of experimental conditions. The conductance of α,ω-alkanedithiols (CnSH) and α,ω-alkanediamines ($CnNH_2$) were measured based on the "stretching-holding" approach (Figure 10a). Both molecules have four distinct molecular conductance features (Figure 10b and c). It is found that these four conductance features have similar decay constants and different contact resistances by measuring alkane chains with different lengths. This indicates that the discrepancy of four conductances originates from the different contact configurations between molecules and electrodes. Further studies were conducted by adding regular AC triangular piezoelectric transducer modulations during the "stretching-holding",[10b] and the concept of contact decay constant β_C is introduced to represent different molecule−electrode contact configurations, which is different from the molecular decay constant β (Figure 10d and e). The contact decay constant β_C can be written as[11a]

$$\beta_C(d) = -\frac{\partial \ln(G)}{\partial(d)} \quad (1)$$

The conductance is differentiated in every half of the oscillation period as shown in Figure 10f; the curve of β_C concerning the extensions Δd can be obtained from eq 1. The variation of the tip−molecule force ΔF concerning Δd can also be calculated. After statistical averaging, $\beta_C-\Delta d$ and $\Delta F-\Delta d$ curves were obtained for these four conductance features. In C8SH junctions, as the rupture force of Au−S bond exceeds Au−Au bond, the mechanical extensions could cause the rearrangement of the gold atoms leading to changes of the contact decay constant β_C. This process confirms the creep mode in which ΔF increases nonlinearly with extensions Δd. The G_{S4} set of C8SH therefore indicates that the molecule may locate in the hollow sites of Au electrodes originally. At the beginning of extensions, the rearrangement of the gold atoms takes place. With the extensions above 0.4 Å, the molecule changes to the top sites of electrodes; further extension could only elongate the Au−S bond in which β_C remains constant and follows the elastic mode where ΔF increases linearly with extensions Δd (Figure 10g). Similar analyses show that the molecule may locate in the top sites of Au electrodes originally for the G_{S1} set of C8SH (Figure 10h). The G_{S4} set of C8SH indicates that the molecule may

https://doi.org/10.1021/acsomega.1c04785
ACS Omega 2021, 6, 30873−30888

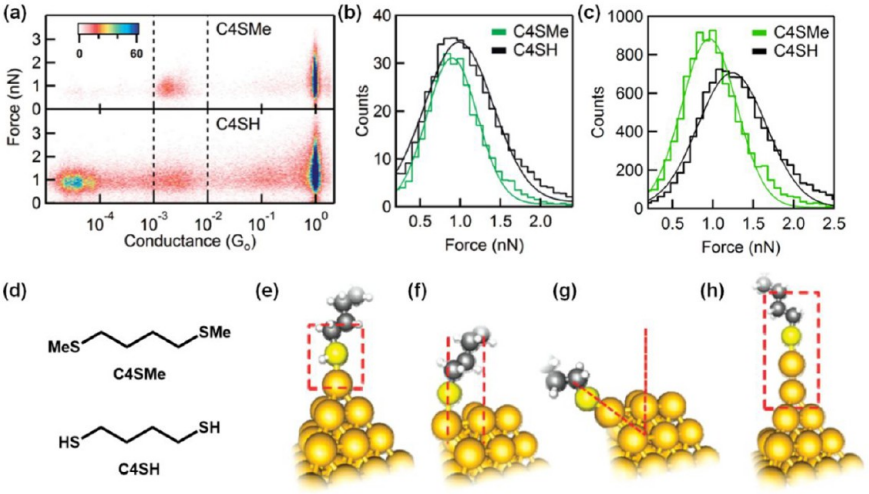

Figure 9. (a) 2D conductance versus force histogram for C4SMe and C4SH. (b) 1D force histogram for C4SMe and C4SH with conductance within the dashed box in (a). (c) 1D force histograms of maximum force events per trace with conductance conform to molecular features for C4SMe and C4SH. (d) Structure of C4SMe and C4SH. (d–g) Possible contact configuration of C4SH with the gold electrode. Adapted from ref 3a. Copyright from 2012 American Chemical Society.

locate in the hollow sites of Au electrodes originally, while the G_{S1} set may indicate the top sites. On the other hand, the rupture force of Au–N bond is below the Au–Au bond, resulting in no rearrangement process; this results in the four conductance features with similar $\beta_C - \Delta d$ and $\Delta F - \Delta d$ curves (Figure 10i).

Combining the controllable mechanical modulations and the cross-correlation analysis, Wang et al. mapped the relationship between conductance and force of the C8SH molecule junctions.[21] Compared with nonmodulated data (Figure 11a), FC-2DCCH for modulated data shows four strong positively related regions consistently for different modulation amplitudes (Figure 11b–d solid line circles), which reflect the conductance and force changes during the intermediate state of two kinds of junction conformations. The two configurations may have different Au–S bond sites, molecular angle tilt, or single-molecule junction length. This change in conductance may result from the variation of the coupling energy between anchor groups and Au. However, if a large enough force is applied, the accompanying large coupling energy change can lead to the change of molecule–electrode adsorption configuration. On the other hand, these discrete regions (Figure 11d dashed line circles) are speculated to be related to the intermediate evolutionary state of single-molecule junctions. Although this study provides a novel approach to analyze the correlation between force and conductance, it is still unable to correlate these related regions of force and conductance with the structure of single-molecule junctions completely.

One of the ultimate goals of molecular electronics is to make effective molecular electronic devices, and one of the parameters that has to be considered is mechanical stability.[22] Although the Au–S bond is widely used in molecular electronics research due to its convenient operation, its nature is still dominated by dispersion force, so its weak strength and poor directional determination make it difficult to be applied in the manufacture of molecular electronic devices.[23] In recent years, contacts based on covalent bonds such as Au–C, Si–C, and Si–S bonds have been studied using STM-BJ.[24] They should have superior conductivity and mechanical stability, but these studies lack direct characterization of their mechanical properties. AFM-BJ is especially suitable for studying these systems, and it can be predicted that AFM-BJ will be widely used in the measurement of mechanical and electrical properties of single-molecule junctions based on covalent bonds in the future.

2.3. Energy Analysis of Molecule–Electrode Interface.

The thermal energy caused by the high current can affect the value of rupture force because of the correlation between energy and force. On the other hand, bond energies can be quantified by integrating the sustaining force.

Current-Induced Local Heating Analysis. Local heating is an important problem to be considered in the design of molecular electronic devices. Although there is no energy exchange between electrons and phonons in coherent transport, local heating can still be generated by a large current density. Huang et al. developed a method for analyzing local heating based on rupture force.[7a] Because chemical bonds have a probability of breaking down due to thermal fluctuations, the rupture force increases with the probe loading rate until a constant value has been reached. However, as the loading rate increases, the contribution due to thermal fluctuations decreases until the adiabatic regime is reached, and the loading rate which had just reached the adiabatic regime was chosen in follow-up experiments to diminish the thermal fluctuations. The most probable rupture force ($\mathbf{F}^*$) can be written as

$$\mathbf{F}^* = \frac{k_B T_{eff}}{x_\beta} \ln\left(\frac{t_{off} x_\beta}{k_B T_{eff}}\right) + \frac{k_B T_{eff}}{x_\beta} \ln r_F \quad (2)$$

where k_B is Boltzmann constant; T_{eff} is the effective local temperature of molecule–electrode interface; x_β is the average length of thermal bonds along the stretch direction until breaking; r_F is the loading rate, and t_{off} is a bond lifetime which can be given by

$$t_{off} = t_D \exp\left(\frac{E_b}{k_B T_{eff}}\right) \quad (3)$$

where t_D is diffusion relaxation time, and E_b is the dissociation activation energy. So, the local temperature can be deduced from the rupture force. When the bias is increased, the rupture force decreases with bias which was attributed to the current-induced heating effect. Under a bias of 1 V, the temperature of the C8SH

https://doi.org/10.1021/acsomega.1c04785
ACS Omega 2021, 6, 30873–30888

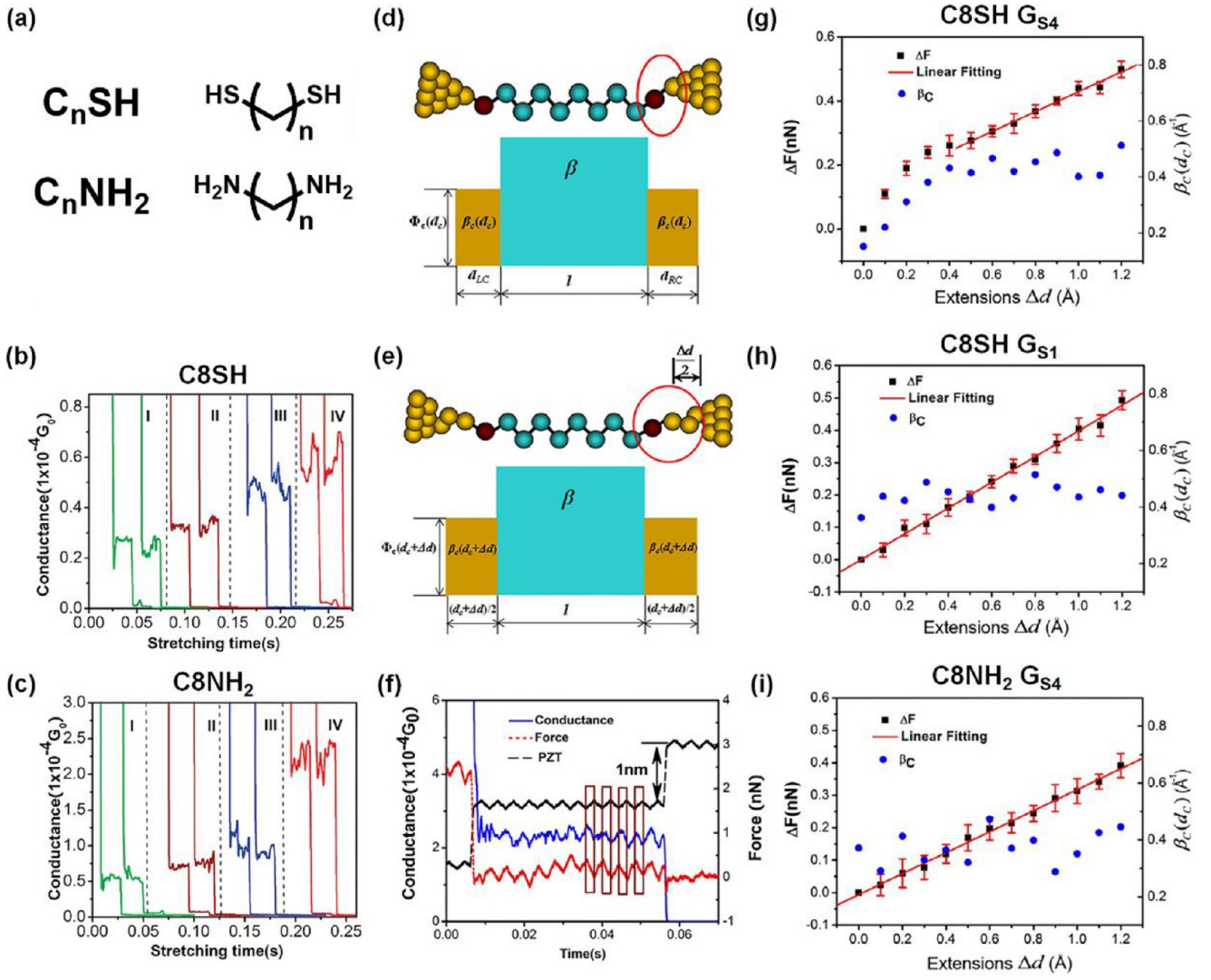

Figure 10. (a) Structures of C8SH and $C8NH_2$. Representative conductance traces for the four features (G_{S1}−G_{S4}) of C8SH (b) and $C8NH_2$ (c). Schematic diagram of energy profile (d) before and (e) after the extension Δd of single-molecule junctions. (f) Conductance (blue) and force (red) trace measured by the controllable mechanical modulations. β_C−Δd and ΔF−Δd curves of G_{S4} (g) and G_{S1} (h) conductance sets for C8SH and G_{S4} conductance sets for $C8NH_2$ (i) single-molecule junctions. Some of the subgraphs are reprinted in part with permission from ref 10a, Copyright 2009 American Chemical Society; ref 10b, copyright 2010 American Chemical Society; ref 11a, Copyright 2011 American Institute of Physics; ref 11b, Copyright from 2012 Institute of Physics.

junction increased by about 30 K relative to room temperature. With the increase of bias voltage, the single-molecule junctions become unstable increasingly.

Bond Energetics Analysis. The force as a function of elongation indicates a mechanical model of the single-molecule junctions. Figure 12a shows the junction stiffness is the first derivative of the rupture force, and the bond energy is the integral of the rupture force for distance. The junction stiffness can be simply measured by calculating the slope of the ramps near the rupture force in force traces.[3c,4a,7b] According to the rules of static equilibrium, the weakest part of the bond determines the limitation of sustainable force, which can associate junction stiffness and the energy of the bond. However, affected by thermal fluctuations, the experimental rupture force is consistent with the maximum sustainable force on the potential energy surface; the measured rupture point still does not reach the asymptotic range of zero interaction energy. The formation and break of the single-molecule junctions would go through a series of structural rearrangements, making it difficult to measure a complete mechanical curve. Aradhya et al. improved the quantitative calculation method of bond energy by presenting a new hybrid model,[7b] that combines the harmonic component (which describes the linear force-to-displacement relationship of the near-equilibrium regime) and the logarithmic component (which describes the nonlinear segment of the bond rupture and the asymptotic zero force regime). By fitting the mechanical curve through this model and integral the force concerning distance, a more accurate bond energy can be obtained. Figure 12 shows some representative traces of Au−Au junction (b and d) and C4SMe−Au junction (c and e) fitted using the hybrid model. Using the optimized model, a series of the binding energy values of bonds were quantified. The results were similar to those calculated by DFT, which proves the correctness of this model.

2.4. Controlling the Molecular Conformation. Taking advantage of tactile-feedback controlled AFM-BJ, the tip−

https://doi.org/10.1021/acsomega.1c04785
ACS Omega 2021, 6, 30873−30888

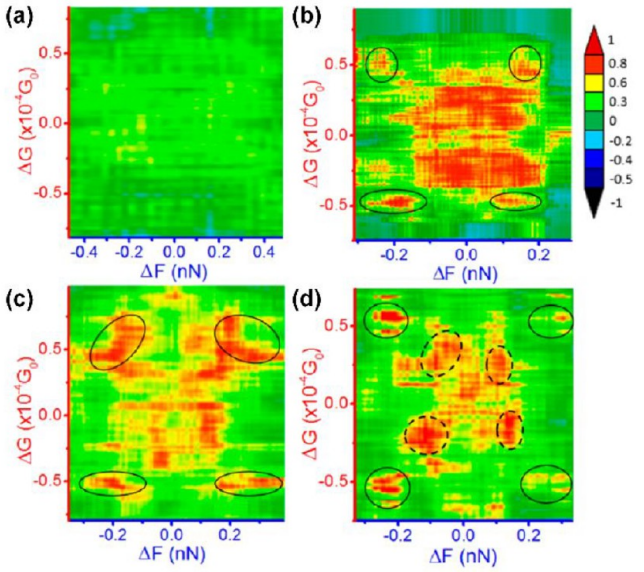

Figure 11. Force-conductance 2D cross-correlation histogram (FC-2DCCH) for nonmodulated data (a) and modulated data (amplitude = 0.8 Å, b; amplitude = 1.0 Å, c; amplitude = 1.2 Å, d). Adapted from ref 21. Copyright from 2014 American Chemical Society.

sample forces can also be quantitatively controlled, which allows the molecular conductance as a function of the tip−sample force. Chen et al. measured the effect of molecular conformation on molecular conductance using C8SH and 1,8-Bis-(diphenylphosphino)octane ($C8PPh_2$).[8] The break junction is realized by a linear increase of tip−sample force rather than displacement (Figure 13a and e). Known from Figure 13b and f, the conductance fluctuation decreases with the increment of tip−sample force which exhibits triangle-shaped occurrence in 2D force versus conductance histogram. The molecule conductance is measured by maintaining the single-molecule junctions with different force values (Figure 13c and g). The fluctuation of conductance decreases significantly with the increase of tensile force, and the peak values of conductance decrease slightly (Figure 13d and h). The reason for this is that as the tensile force increases, the conformation of the alkane chain changes from gauche to all-trans conformer, which leads to the decrease of conductance fluctuation. Meanwhile, the defects of the gauche conformer create coupling between spatially adjacent methylene units and cause a through-space pathway, which leads to the conductance of gauche higher than that of all-trans. This study achieves the control of molecular conformation to some degree, which is of great significance.

3. THEORETICAL STUDIES

The theoretical research prior to the experiment is of great significance, providing guidelines for the subsequent experimental research. This has also stimulated some theoretical research attempts in this area.

The change of structure is inevitably accompanied by the change of mechanical properties, indicating a correlation between force and conductance.[25] Franco et al. studied the change of force and conductance of PDI−PY based on molecular dynamics (MD) simulations and tight-binding methods. The structure of PDI−PY is shown in Figure 14a, which is easy to make conformational change.[26] Specifically, a folded conformation includes a $\pi-\pi$ stacking interaction resulting in higher conductivity, and stretching results in an extended conformation that reduces the conductance by several orders of magnitude. Figure 14b shows the change of force and transmission during pulling where L is the distance between the cantilever and the substrate; both force and transmission have significant variations around 23 Å. Transmission was also studied as a function of molecular length ξ (Figure 14c). Both Hückel IV and gDFTB methods indicate a similar trend in which transmission drops rapidly near 22 Å. These changes correspond to the unfolded conformation of PDI−PY. The local transmission elements were calculated, and a quantitative diagram of the contribution of local transmission to total transmission was plotted as Figure 14c, which is highlighted if the local transmission contribution associated with the conformation accounts for more than 80% of the total transmission. At shorter molecular length ξ, the transport is mainly based on $\pi-\pi$ stacking interaction (red points) and quadruple hydrogen bonds (green points). As the molecule elongates, a new hydrogen bond

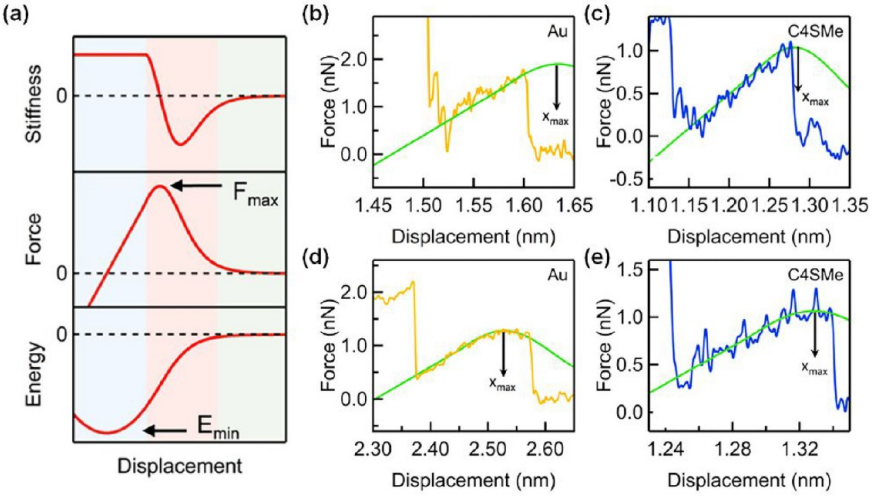

Figure 12. (a) Schematic diagram of the potential energy, force, and stiffness as a function of elongation. (b−e) Representative force traces of Au−Au junction (b and d) and C4SMe−Au junction (c and e) fitted using the hybrid model. Adapted from ref 7b. Copyright from 2014 American Chemical Society.

https://doi.org/10.1021/acsomega.1c04785
ACS Omega 2021, 6, 30873−30888

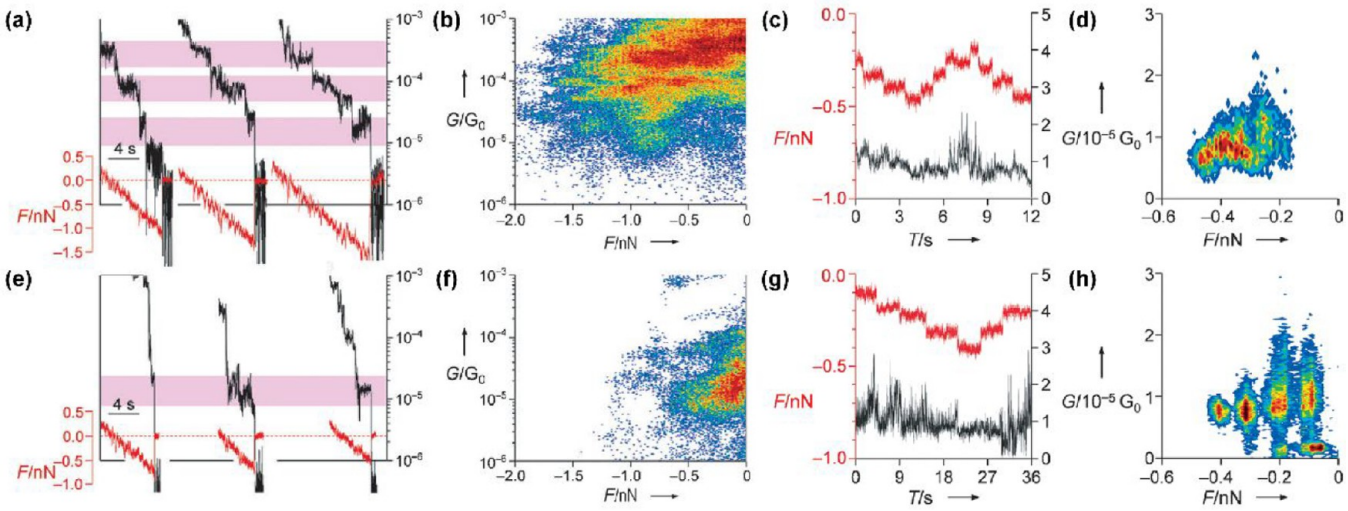

Figure 13. Conductance distributions of C8SH (a–d) and C8PPh$_2$ (e–h). (a, e) Force and conductance traces. (b, f) 2D force versus conductance histogram. (c, d, g, h) Conductance response as a function of tip–sample force. Adapted with permission from ref 8. Copyright from 2013 WILEY-VCH Verlag GmbH & Co. KGaA, Weinheim.

is formed at $\xi \approx 21$ Å, which plays a significant role in transmission (purple points). The continuous elongating results in the weakening of the $\pi-\pi$ stacking and the destruction of the hydrogen bond, which performs the decrement of transmission. When stretched beyond 23 Å, again, a new hydrogen bond is formed gradually, causing the increment of transmission (blue points).

Another interesting molecule that has the cyclophane structure (Figure 15a, cyc-PH) was also investigated subsequently.[27] As shown in Figure 14a, cyc-PH shows an abnormal increase in molecular conductance as the molecule elongates (Figure 15b). This is because the molecular structure has transport-determining electronic couplings, which can be enhanced by applying force. In 2017, Pirrotta et al. investigated the force-conductance spectrum of two hydrogen bonding complexes (Figure 15a, Hydro C and Hydro O).[28] As depicted in Figure 15c and d, with the change of chemical structure, the force-conductance spectrum shows a variety of changes, which promises to be a fingerprint that can identify subtle changes in molecular structure during break junctions.

Chemical reactions at the single-molecule scale are obviously different from the macroscopic scale, which makes this research a hot topic, but the lack of characterization limits further development. The mechanical and electrical properties of single-molecule junctions varied after chemical reactions, resulting in force-conductance spectroscopy becoming a potential tool for studying chemical reactions at the single-molecule scale. In 2019, Mejía et al. studied the isomerization of cyclopropane oligomers using force-conductance spectroscopy.[29] The cyclopropane oligomer (cyc-C3, Figure 16a) was fixed on graphene nanoribbon (GNR) electrodes. As shown in Figure 16b and c, three regions appear in both force and transmission distribution denoted as I, II, and III. Cyclic isomerization occurs in region II, which shows a marked change. The correlation between force and conductance signals provides a new idea for the characterization of chemical reactions at the single molecular scale, allowing reactants, products, and intermediates or even small conformational changes to be differentiated. Recently, Mejía et al. studied Diels–Alder (DA) reaction theoretically.[30] The results show that the reactivity can be controlled by changing the distance between electrodes and the activation energy decreases at low temperatures. Meanwhile, the formation of reaction products also leads to the increase of conductance. These allow the reaction to be mechanically regulated and simultaneously characterized by AFM-BJ.

4. OTHER COMPLEMENTARY TECHNIQUES

Although most studies to measure the mechanical and electrical properties of single-molecule junctions use AFM-BJ, the researchers developed various other techniques to measure these properties, which provide an additional perspective on molecular junctions and allow us to more fully understand the correlations of their electrical and mechanical properties in the evolution of single-molecule junctions.

Rascón-Ramos et al. applied a small-amplitude high-frequency sinusoidal mechanical oscillation based on STM-BJ technique (Figure 17a).[31] The tunneling current can usually be expressed as

$$I(z) = VG_C\, e^{-\beta z} \tag{4}$$

where V stands for the bias between the electrodes, G_C is contact conductance, β represents the tunnelling decay constant, and z is the electrode spacing. In the case that mechanical oscillations were added, z can be expressed by $z = z_0 + A_0 \cos \omega t$, and by performing a Taylor expansion of the above equation around $Z_0 = L$, eq 5 can be obtained:

$$I \cong I_{DC} + \frac{dI_{DC}}{dz}\bigg|_L A_0 \cos \omega t + \ldots \tag{5}$$

where the first term is DC magnitude which can be expressed as $I_{DC}(L) = VG_C\, e^{-\beta z}$, and the second term is AC magnitude (I_{AC}). A value called α can be given by $\alpha = I_{AC}/(A_0 \times I_{DC})$. By comparing the measurements of C6SH and mC6SH (Figure 17f), it can be found that the α and β values of mC6SH, which only has the tunneling current, are almost equal (Figure 17b and c). Alternatively, the α and β values of C6SH are quite different (Figures 17d and e). Through control experiments, it is concluded that the difference between the two values stems from the mechanical properties of molecular junctions. Based on the fact that most of the applied amplitude is absorbed by the gold contact region, the actual amplitude of mechanical

https://doi.org/10.1021/acsomega.1c04785
ACS Omega 2021, 6, 30873−30888

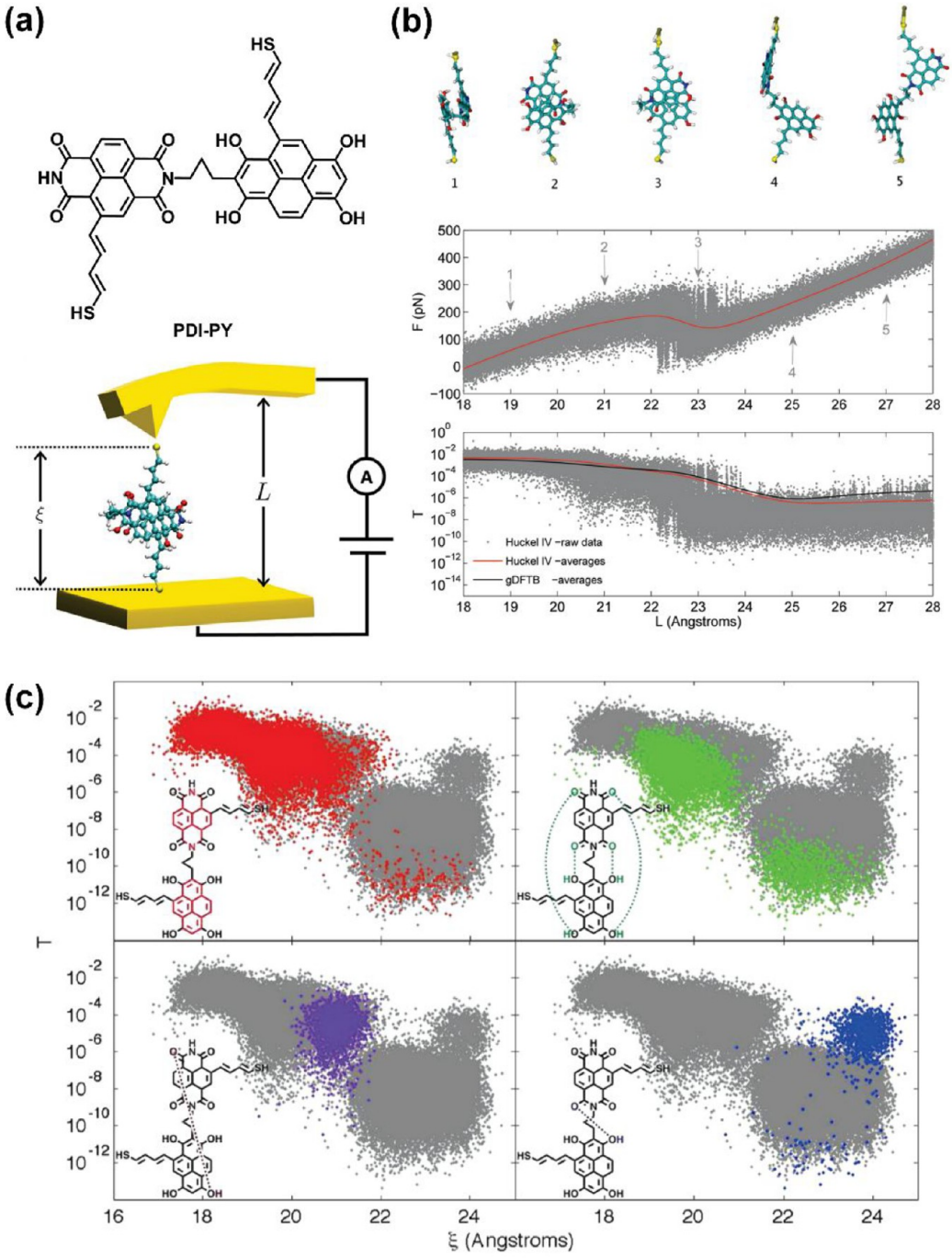

Figure 14. (a) Structures of PDI−PY and schematic diagram of the single-molecule junction. (b) Snapshot of molecular structure changes and average force and transmission during junction stretching. (c) Conformational properties in the charge transport. The dots are highlighted if the local transmission of a conformation contributes more than 80% of the total transmission. Adapted from ref 26. Copyright 2011 American Chemical Society.

oscillation A_{jxn} has the following relation: $\alpha/\beta = A_{jxn}/A_0$. By combining density functional theory (DFT), molecular dynamics (MD) modules, and a reasonable mechanical model of the single-molecule junction (Figure 17g), the most suitable single-molecule junction structure can be obtained in which the thiol anchoring groups are both on the top site, while the apex gold atoms of the two electrodes are on the top site and bridge site, respectively.

In 2018, Ramachandran et al. extended this method to measure molecules with aromatic rings (Figure 18a).[32] Different from alkanedithiols, the thiol is an electron-withdrawing group relative to the phenyl ring, which causes a discrepancy in binding energy of the thiol group to the gold atom. This results in the phenomenon in which oligophenylene-dithiol molecules have two significantly different conductance values. The α values of the low-conductance states have a similar change of alkanedithiols (Figure 18c upper panel), indicating that a simple mechanical model can describe the results and provide a configuration as shown in Figure 18b (Config. A). However, the high-conductance states have a lower value of α (Figure 18c lower panel), and a more complex model is needed. It is assumed that the phenyl overlaps with the gold electrodes and the

https://doi.org/10.1021/acsomega.1c04785
ACS Omega 2021, 6, 30873−30888

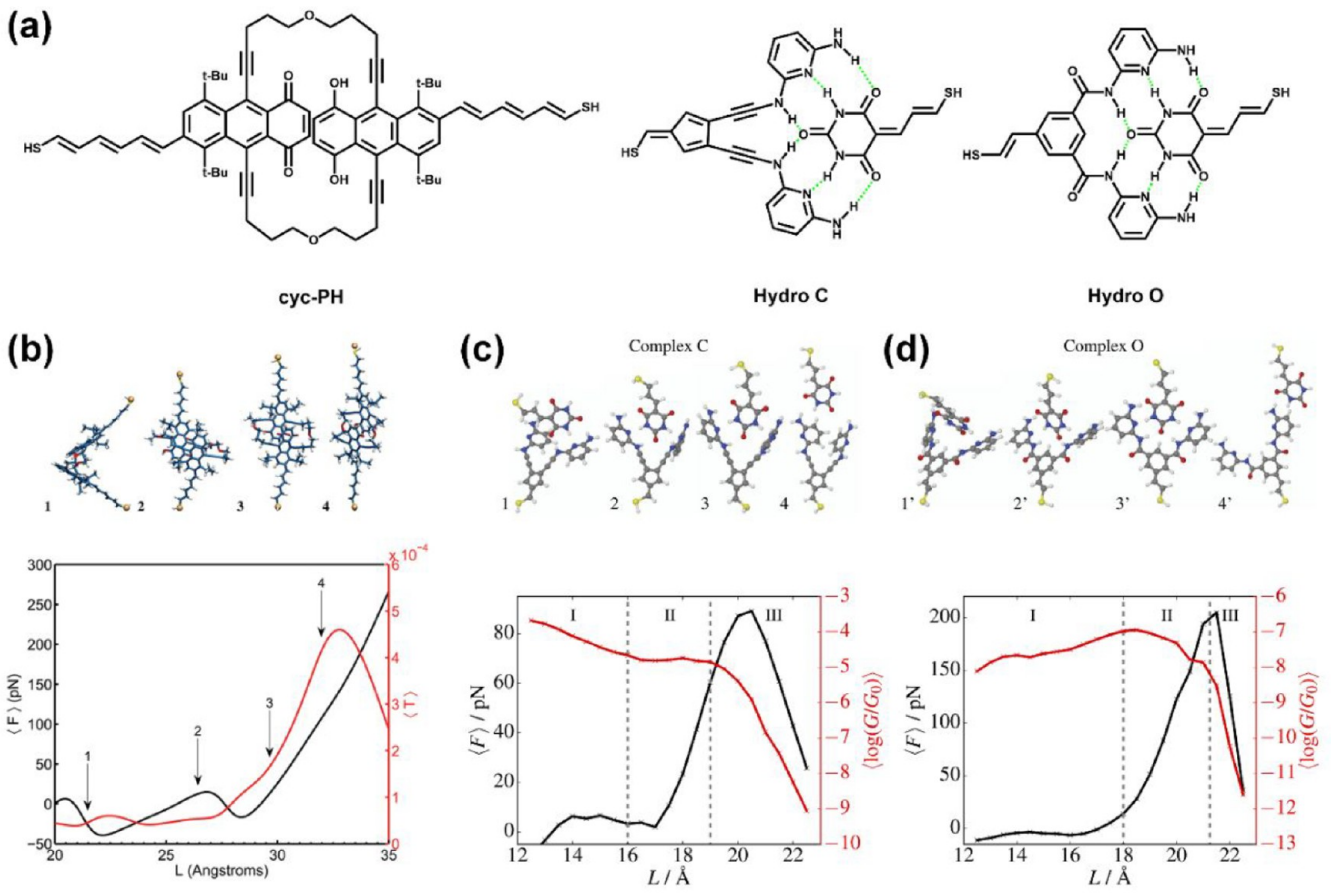

Figure 15. (a) Structures of cyc-PH, Hydro C, and Hydro O. Snapshot of molecular structure changes and average force and transmission (or conductance) during junction stretching for cyc-PH (b), Hydro C (c), and Hydro O (d). Some of the subgraphs are reprinted in part with permission from ref 27, copyright 2011 American Chemical Society; from ref 28, copyright 2017 American Institute of Physics.

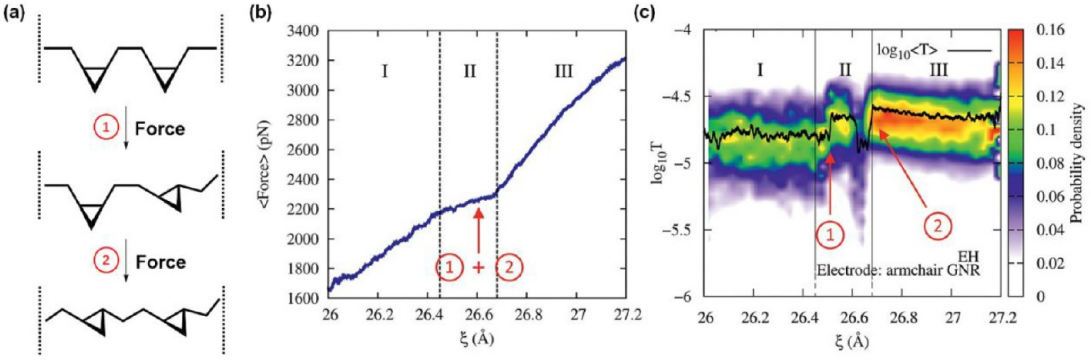

Figure 16. (a) Structures of cyc-C3. Average force (b) and transmission (c) during stretching. Adapted with permission from ref 29. Copyright from 2011 the Royal Society of Chemistry.

molecules only slip along the electrode, resulting in a change in the area of overlap between the π orbital and the gold electrode as shown in Figure 18b, which is consistent with the experiment results (Config. B). This method provides insights into the origin of polydispersity of molecular conductance and provides more accurate single-molecule junction models, which lays a foundation for further exploration of molecule-electronic devices.

The break junction technique is a statistical method, the advantage of which is performing many experiments in a short space of time and obtaining the properties of single-molecule junctions through statistical analysis. However, this in turn limits the precise insight into the specific configuration and the dynamic change of the conformation of single-molecule junctions. Scanning tunneling and atomic force microscopy (STM/AFM) pulling experiments (Figure 19a)[33] overcome these shortcomings. In 2009, Lafferentz et al. studied the electrical properties of poly-DBTF (Figure 19a) by STM pulling. Poly-DBTF was prepared by in situ polymerization, and the end of molecular wire could be found by STM imaging. The AFM tip was positioned at one end and established electronic contact with the molecule. Then the molecular wire was

https://doi.org/10.1021/acsomega.1c04785
ACS Omega 2021, 6, 30873−30888

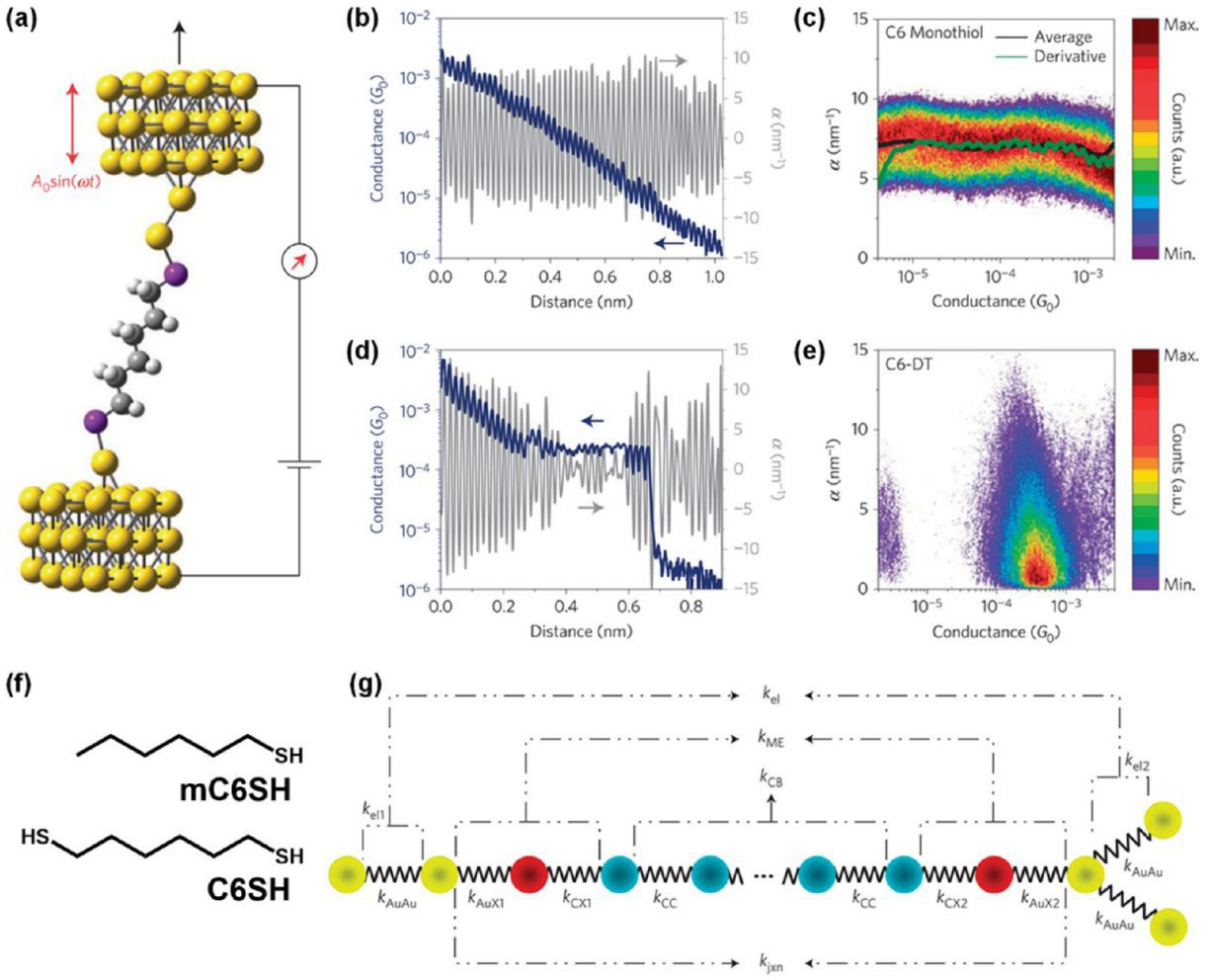

Figure 17. (a) Schematic diagram of the experimental setup. Representative curve of current versus distance (blue curve) and normalized current (α) at the oscillation frequency (2 kHz) for mC6SH (b) and C6SH (d). 2D histogram extracted from thousands of current versus distance traces for mC6SH (c) and C6SH (e). (f) Structures of mC6SH and C6SH. (g) Mechanical model of single-molecule junction. Adapted with permission from ref 31. Copyright 2015 Springer Nature.

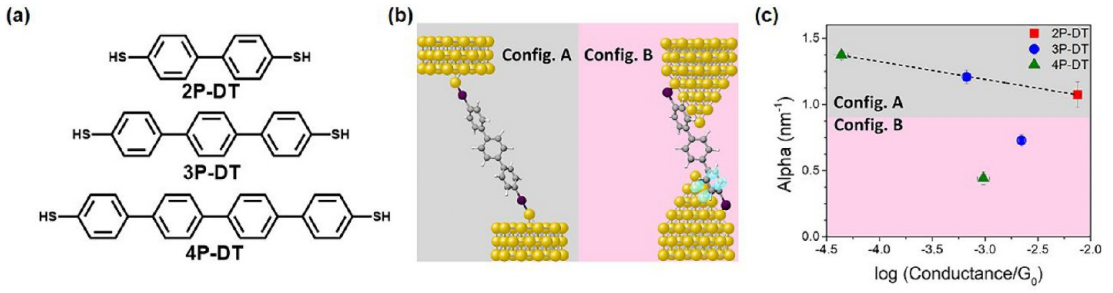

Figure 18. (a) Structures of 2P-DT, 3P-DT, and 4P-DT. (b) Schematic diagram of configurations of 3P-DT in break junctions. (c) Plot of α versus conductance for the two configurations of 2P-DT, 3P-DT, and 4P-DT. Config. A for gray panel and Config. B for pink panel. Adapted from ref 32. Copyright 2018 American Chemical Society.

gradually pulled away from the Au(111) surface. The conductance G which is obviously higher than the vacuum gap at a 0.1 V bias was recorded as a function of the distance z between the tip and the surface. The conductance curve decays not completely linearly, but a characteristic oscillation occurs at a particular stretch distance (Figure 19b). It is speculated that the maximum of this oscillation comes from the monomer units adsorbed from the surface being detached gradually. In 2014, Kawai et al. further investigated poly-DBTF based on AFM equipped with a tuning-fork piezoelectric sensor. The sensor will oscillate at a certain frequency through mechanical excitation. The measured frequency shift Δf can reflect the force gradient k_{st} of the tip−sample interaction. The molecular wire was pulled away from the surface similarly, and a periodic jump of Δf is observed. The average step distance is 0.91 ± 0.07 nm, similar to the length of the monomer unit (0.845 nm), verifying that the molecular wire was detached from the surface unit by unit. Based on the Frenkel−Kontorova (FK) model, it can be theoretically

https://doi.org/10.1021/acsomega.1c04785
ACS Omega 2021, 6, 30873−30888

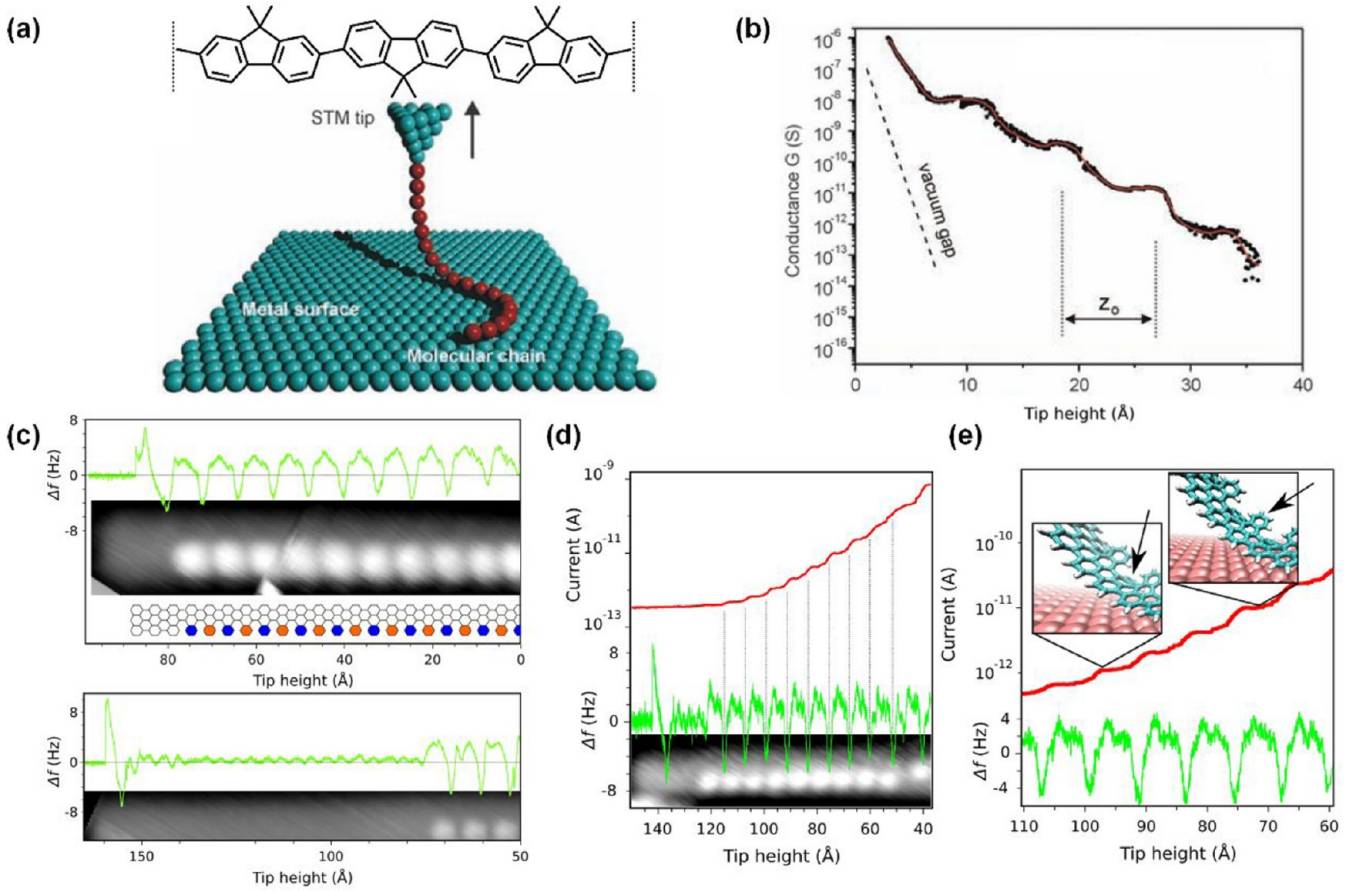

Figure 19. (a) Structure of poly-DBTF. (b) Schematic diagram of experimental setup. (b) Trace of tip height versus conductance. (c) Trace of tip height versus Δf and STM image of graphene nanoribbons (GNRs) with defects. The bias is 0 and 0.8 V for upper and lower, respectively. (d) Curves of conductance and Δf for GNRs with the change of tip height during pulling. (e) Magnification of (d) with insets showing the detaching process. Some of the subgraphs are reprinted in part with permission from ref 33a, Copyright 2009 American Association for the Advancement of Science; from ref 34, Copyright 2018 American Physical Society.

concluded that k_{st} also has similar periodic changes and predicted the components of lateral force and normal force. The adsorption energy can be extracted by quantifying the difference between the work done by the tip and the energy dissipation. In 2018, Koch et al. studied graphene nanoribbon (GNR) defects combining STM and AFM pulling,[34] which permit a simultaneous electrical and mechanical characterization of the molecular wire. As shown in Figure 19c, structural defects exist in non-fully dehydrogenated ribbons, which emerge as a highlight in STM images. The period of Δf fits well with the length of a dianthracene unit, and Δf changes significantly only in the defective positions, while weak changes were observed in the defect-free units. All the features suggested that each period corresponds to a unit of defect in ribbons. The addition of bias makes it possible to measure conductance simultaneously (Figure 19d). The features of current and Δf can be divided into two parts: the more strongly bound unit detached causes a negative peak of Δf and decreasing current feature, while the weakly bound unit results in a positive peak of Δf and constant current feature (Figure 19e).

5. CONCLUSIONS

In this mini-review, we summarized the research progress using the AFM-BJ technique. Briefly, the rupture force of single-molecule junctions and even single-supramolecule junctions can be analyzed, the configuration evolution process can be mapped through force and conductance correlation analysis, and the energy of the molecule−electrode interface can be quantized, and even molecular conformation can be regulated to some extent utilizing controlling tip−sample force. However, satisfying the simultaneous measurement of force and conductance signals also limits the improvement of signal-to-noise ratio, and the development of targeted data analysis methods is still a key point.

As a perspective, AFM-BJ technique is essentially the intersection of molecular electronics and molecular mechanics, which provides a unique platform. It may become an important method to characterize the stability of molecular electronic devices and the chemical reactions in single-molecule level, and we hope that it can be further extended to the measurement of the electromechanical properties of supramolecular systems, which can shed new light on the nature of supramolecular interactions. This may be a powerful tool for characterizing novel phenomena at the single-molecule level.

AUTHOR INFORMATION

Corresponding Authors

Wenjing Hong − *State Key Laboratory of Physical Chemistry of Solid Surfaces, iChEM, NEL, College of Chemistry and Chemical Engineering, Xiamen University, Xiamen 361005,*

https://doi.org/10.1021/acsomega.1c04785
ACS Omega 2021, 6, 30873−30888

China; orcid.org/0000-0003-4080-6175; Email: whong@xmu.edu.cn

Zhibing Tan − *State Key Laboratory of Physical Chemistry of Solid Surfaces, iChEM, NEL, College of Chemistry and Chemical Engineering, Xiamen University, Xiamen 361005, China*; Email: tanzhibing@xmu.edu.cn

Author

Yixuan Zhu − *State Key Laboratory of Physical Chemistry of Solid Surfaces, iChEM, NEL, College of Chemistry and Chemical Engineering, Xiamen University, Xiamen 361005, China*

Complete contact information is available at: https://pubs.acs.org/10.1021/acsomega.1c04785

Notes

The authors declare no competing financial interest.

■ ACKNOWLEDGMENTS

This work was supported by Natural Science Foundation of China (nos. 21722305, 21673195 and 21703188), the China Postdoctoral Science Foundation (no. 2017M622060), the National Key R&D Program of China (nos. 2017YFA0204902) and the Beijing National Laboratory for Molecular Sciences (no. BNLMS202005).

■ REFERENCES

(1) Aviram, A.; Ratner, M. A. Molecular Rectifiers. *Chem. Phys. Lett.* **1974**, *29* (2), 277−283.

(2) (a) Jia, C.; Migliore, A.; Xin, N.; Huang, S.; Wang, J.; Yang, Q.; Wang, S.; Chen, H.; Wang, D.; Feng, B.; Liu, Z.; Zhang, G.; Qu, D.-H.; Tian, H.; Ratner, M. A.; Xu, H. Q.; Nitzan, A.; Guo, X. Covalently Bonded Single-Molecule Junctions with Stable and Reversible Photoswitched Conductivity. *Science* **2016**, *352* (6292), 1443−1445. (b) Yang, C.; Liu, Z.; Li, Y.; Zhou, S.; Lu, C.; Guo, Y.; Ramirez, M.; Zhang, Q.; Li, Y.; Liu, Z.; Houk, K. N.; Zhang, D.; Guo, X. Electric Field−Catalyzed Single-Molecule Diels-Alder Reaction Dynamics. *Sci. Adv.* **2021**, *7* (4), eabf0689. (c) Tan, Z.; Zhang, D.; Tian, H.-R.; Wu, Q.; Hou, S.; Pi, J.; Sadeghi, H.; Tang, Z.; Yang, Y.; Liu, J.; Tan, Y.-Z.; Chen, Z.-B.; Shi, J.; Xiao, Z.; Lambert, C.; Xie, S.-Y.; Hong, W. Atomically Defined Angstrom-Scale All-Carbon Junctions. *Nat. Commun.* **2019**, *10* (1), 1748. (d) Bai, J.; Daaoub, A.; Sangtarash, S.; Li, X.; Tang, Y.; Zou, Q.; Sadeghi, H.; Liu, S.; Huang, X.; Tan, Z.; Liu, J.; Yang, Y.; Shi, J.; Mészáros, G.; Chen, W.; Lambert, C.; Hong, W. Anti-Resonance Features of Destructive Quantum Interference in Single-Molecule Thiophene Junctions Achieved by Electrochemical Gating. *Nat. Mater.* **2019**, *18* (4), 364−369. (e) Zhao, Z.; Guo, C.; Ni, L.; Zhao, X.; Zhang, S.; Xiang, D. In Situ Photoconductivity Measurements of Imidazole in Optical Fiber Break-Junctions. *Nanoscale Horiz.* **2021**, *6* (5), 386−392. (f) Zang, Y.; Zou, Q.; Fu, T.; Ng, F.; Fowler, B.; Yang, J.; Li, H.; Steigerwald, M. L.; Nuckolls, C.; Venkataraman, L. Directing Isomerization Reactions of Cumulenes with Electric Fields. *Nat. Commun.* **2019**, *10* (1), 4482. (g) Carlotti, M.; Soni, S.; Kumar, S.; Ai, Y.; Sauter, E.; Zharnikov, M.; Chiechi, R. C. Two-Terminal Molecular Memory through Reversible Switching of Quantum Interference Features in Tunneling Junctions. *Angew. Chem., Int. Ed.* **2018**, *57* (48), 15681−15685. (h) Aragonès, A. C.; Haworth, N. L.; Darwish, N.; Ciampi, S.; Bloomfield, N. J.; Wallace, G. G.; Diez-Perez, I.; Coote, M. L. Electrostatic Catalysis of a Diels−Alder Reaction. *Nature* **2016**, *531* (7592), 88−91. (i) Ciampi, S.; Darwish, N.; Aitken, H. M.; Díez-Pérez, I.; Coote, M. L. Harnessing Electrostatic Catalysis in Single Molecule, Electrochemical and Chemical Systems: a Rapidly Growing Experimental Tool Box. *Chem. Soc. Rev.* **2018**, *47* (14), 5146−5164. (j) Jiang, F.; Trupp, D. I.; Algethami, N.; Zheng, H.; He, W.; Alqorashi, A.; Zhu, C.; Tang, C.; Li, R.; Liu, J.; Sadeghi, H.; Shi, J.; Davidson, R.; Korb, M.; Sobolev, A. N.; Naher, M.; Sangtarash, S.; Low, P. J.; Hong, W.; Lambert, C. J. Turning the Tap: Conformational Control of Quantum Interference to Modulate Single-Molecule Conductance. *Angew. Chem., Int. Ed.* **2019**, *58* (52), 18987−18993. (k) Capozzi, B.; Xia, J.; Adak, O.; Dell, E. J.; Liu, Z.-F.; Taylor, J. C.; Neaton, J. B.; Campos, L. M.; Venkataraman, L. Single-Molecule Diodes with High Rectification Ratios through Environmental Control. *Nat. Nanotechnol.* **2015**, *10* (6), 522−527.

(3) (a) Frei, M.; Aradhya, S. V.; Hybertsen, M. S.; Venkataraman, L. Linker Dependent Bond Rupture Force Measurements in Single-Molecule Junctions. *J. Am. Chem. Soc.* **2012**, *134* (9), 4003−4006. (b) Meisner, J. S.; Ahn, S.; Aradhya, S. V.; Krikorian, M.; Parameswaran, R.; Steigerwald, M.; Venkataraman, L.; Nuckolls, C. Importance of Direct Metal−π Coupling in Electronic Transport Through Conjugated Single-Molecule Junctions. *J. Am. Chem. Soc.* **2012**, *134* (50), 20440−20445. (c) Aradhya, S. V.; Frei, M.; Hybertsen, M. S.; Venkataraman, L. Van der Waals Interactions at Metal/Organic Interfaces at the Single-Molecule Level. *Nat. Mater.* **2012**, *11* (10), 872−876.

(4) (a) Xu, B.; Xiao, X.; Tao, N. J. Measurements of Single-Molecule Electromechanical Properties. *J. Am. Chem. Soc.* **2003**, *125* (52), 16164−16165. (b) Frei, M.; Aradhya, S. V.; Koentopp, M.; Hybertsen, M. S.; Venkataraman, L. Mechanics and Chemistry: Single Molecule Bond Rupture Forces Correlate with Molecular Backbone Structure. *Nano Lett.* **2011**, *11* (4), 1518−1523.

(5) Rubio, G.; Agraït, N.; Vieira, S. Atomic-Sized Metallic Contacts: Mechanical Properties and Electronic Transport. *Phys. Rev. Lett.* **1996**, *76* (13), 2302−2305.

(6) Ahn, S.; Aradhya, S. V.; Klausen, R. S.; Capozzi, B.; Roy, X.; Steigerwald, M. L.; Nuckolls, C.; Venkataraman, L. Electronic Transport and Mechanical Stability of Carboxyl Linked Single-Molecule Junctions. *Phys. Chem. Chem. Phys.* **2012**, *14* (40), 13841−13845.

(7) (a) Huang; Xu; Chen; Ventra, M. D.; Tao. Measurement of Current-Induced Local Heating in a Single Molecule Junction. *Nano Lett.* **2006**, *6* (6), 1240−1244. (b) Aradhya, S. V.; Nielsen, A.; Hybertsen, M. S.; Venkataraman, L. Quantitative Bond Energetics in Atomic-Scale Junctions. *ACS Nano* **2014**, *8* (7), 7522−7530.

(8) Chen, I.-W. P.; Tseng, W.-H.; Gu, M.-W.; Su, L.-C.; Hsu, C.-H.; Chang, W.-H.; Chen, C.-h. Tactile-Feedback Stabilized Molecular Junctions for the Measurement of Molecular Conductance. *Angew. Chem., Int. Ed.* **2013**, *52* (9), 2449−2453.

(9) Magyarkuti, A.; Adak, O.; Halbritter, A.; Venkataraman, L. Electronic and Mechanical Characteristics of Stacked Dimer Molecular Junctions. *Nanoscale* **2018**, *10* (7), 3362−3368.

(10) (a) Zhou, J.; Chen, F.; Xu, B. Fabrication and Electronic Characterization of Single Molecular Junction Devices: A Comprehensive Approach. *J. Am. Chem. Soc.* **2009**, *131* (30), 10439−10446. (b) Zhou, J.; Chen, G.; Xu, B. Probing the Molecule−Electrode Interface of Single-Molecule Junctions by Controllable Mechanical Modulations. *J. Phys. Chem. C* **2010**, *114* (18), 8587−8592.

(11) (a) Zhou, J.; Xu, B. Determining Contact Potential Barrier Effects on Electronic Transport in Single Molecular Junctions. *Appl. Phys. Lett.* **2011**, *99* (4), 042104. (b) Zhou, J.; Guo, C.; Xu, B. Electron Transport Properties of Single Molecular Junctions under Mechanical Modulations. *J. Phys.: Condens. Matter* **2012**, *24* (16), 164209.

(12) Aradhya, S. V.; Meisner, J. S.; Krikorian, M.; Ahn, S.; Parameswaran, R.; Steigerwald, M. L.; Nuckolls, C.; Venkataraman, L. Dissecting Contact Mechanics from Quantum Interference in Single-Molecule Junctions of Stilbene Derivatives. *Nano Lett.* **2012**, *12* (3), 1643−1647.

(13) Zhou, C.; Li, X.; Gong, Z.; Jia, C.; Lin, Y.; Gu, C.; He, G.; Zhong, Y.; Yang, J.; Guo, X. Direct Observation of Single-Molecule Hydrogen-Bond Dynamics with Single-Bond Resolution. *Nat. Commun.* **2018**, *9* (1), 807.

(14) Yoshida, K.; Pobelov, I. V.; Manrique, D. Z.; Pope, T.; Mészáros, G.; Gulcur, M.; Bryce, M. R.; Lambert, C. J.; Wandlowski, T. Correlation of Breaking Forces, Conductances and Geometries of Molecular Junctions. *Sci. Rep.* **2015**, *5* (1), 9002.

(15) (a) Chen, F.; Li, X.; Hihath, J.; Huang, Z.; Tao, N. Effect of Anchoring Groups on Single-Molecule Conductance: Comparative Study of Thiol-, Amine-, and Carboxylic-Acid-Terminated Molecules. *J. Am. Chem. Soc.* **2006**, *128* (49), 15874−15881. (b) Kim, Y.-H.; Kim, H. S.; Lee, J.; Tsutsui, M.; Kawai, T. Stretching-Induced Conductance Variations as Fingerprints of Contact Configurations in Single-Molecule Junctions. *J. Am. Chem. Soc.* **2017**, *139* (24), 8286−8294.
(16) Hamill, J. M.; Wang, K.; Xu, B. Force and Conductance Molecular Break Junctions with Time Series Crosscorrelation. *Nanoscale* **2014**, *6* (11), 5657−5661.
(17) Haiss, W.; Nichols, R. J.; van Zalinge, H.; Higgins, S. J.; Bethell, D.; Schiffrin, D. J. Measurement of Single Molecule Conductivity Using the Spontaneous Formation of Molecular Wires. *Phys. Chem. Chem. Phys.* **2004**, *6* (17), 4330−4337.
(18) Li, X.; He, J.; Hihath, J.; Xu, B.; Lindsay, S. M.; Tao, N. Conductance of Single Alkanedithiols: Conduction Mechanism and Effect of Molecule−Electrode Contacts. *J. Am. Chem. Soc.* **2006**, *128* (6), 2135−2141.
(19) Nef, C.; Frederix, P. L. T. M.; Brunner, J.; Schönenberger, C.; Calame, M. Force−Conductance Correlation in Individual Molecular Junctions. *Nanotechnology* **2012**, *23* (36), 365201.
(20) Xu, B. Modulating the Conductance of a Au−octanedithiol−Au Molecular Junction. *Small* **2007**, *3* (12), 2061−2065.
(21) Wang, K.; Hamill, J. M.; Zhou, J.; Xu, B. Mapping the Details of Contact Effect of Modulated Au-Octanedithiol-Au Break Junction by Force−Conductance Cross-Correlation. *J. Am. Chem. Soc.* **2014**, *136* (50), 17406−17409.
(22) Hines, T.; Díez-Pérez, I.; Nakamura, H.; Shimazaki, T.; Asai, Y.; Tao, N. Controlling Formation of Single-Molecule Junctions by Electrochemical Reduction of Diazonium Terminal Groups. *J. Am. Chem. Soc.* **2013**, *135* (9), 3319−3322.
(23) Pla-Vilanova, P.; Aragonès, A. C.; Ciampi, S.; Sanz, F.; Darwish, N.; Diez-Perez, I. The Spontaneous Formation of Single-Molecule Junctions via Terminal Alkynes. *Nanotechnology* **2015**, *26* (38), 381001.
(24) (a) Dief, E. M.; Darwish, N. Ultrasonic Generation of Thiyl Radicals: A General Method of Rapidly Connecting Molecules to a Range of Electrodes for Electrochemical and Molecular Electronics Applications. *ACS Sensors* **2021**, *6* (2), 573−580. (b) Walkey, M. C.; Peiris, C. R.; Ciampi, S.; C. Aragonès, A.; Domínguez-Espíndola, R. B.; Jago, D.; Pulbrook, T.; Skelton, B. W.; Sobolev, A. N.; Díez Pérez, I.; Piggott, M. J.; Koutsantonis, G. A.; Darwish, N. Chemically and Mechanically Controlled Single-Molecule Switches Using Spiropyrans. *ACS Appl. Mater. Interfaces* **2019**, *11* (40), 36886−36894. (c) Peiris, C. R.; Ciampi, S.; Dief, E. M.; Zhang, J.; Canfield, P. J.; Le Brun, A. P.; Kosov, D. S.; Reimers, J. R.; Darwish, N. Spontaneous S−Si Bonding of Alkanethiols to Si(111)−H: Towards Si−Molecule−Si Circuits. *Chem. Sci.* **2020**, *11* (20), 5246−5256. (d) Peiris, C. R.; Vogel, Y. B.; Le Brun, A. P.; Aragonès, A. C.; Coote, M. L.; Díez-Pérez, I.; Ciampi, S.; Darwish, N. Metal−Single-Molecule−Semiconductor Junctions Formed by a Radical Reaction Bridging Gold and Silicon Electrodes. *J. Am. Chem. Soc.* **2019**, *141* (37), 14788−14797.
(25) (a) Paulsson, M.; Krag, C.; Frederiksen, T.; Brandbyge, M. Conductance of Alkanedithiol Single-Molecule Junctions: A Molecular Dynamics Study. *Nano Lett.* **2009**, *9* (1), 117−121. (b) Mejía, L.; Renaud, N.; Franco, I. Signatures of Conformational Dynamics and Electrode-Molecule Interactions in the Conductance Profile During Pulling of Single-Molecule Junctions. *J. Phys. Chem. Lett.* **2018**, *9* (4), 745−750.
(26) Franco, I.; George, C. B.; Solomon, G. C.; Schatz, G. C.; Ratner, M. A. Mechanically Activated Molecular Switch through Single-Molecule Pulling. *J. Am. Chem. Soc.* **2011**, *133* (7), 2242−2249.
(27) Franco, I.; Solomon, G. C.; Schatz, G. C.; Ratner, M. A. Tunneling Currents That Increase with Molecular Elongation. *J. Am. Chem. Soc.* **2011**, *133* (39), 15714−15720.
(28) Pirrotta, A.; De Vico, L.; Solomon, G. C.; Franco, I. Single-Molecule Force-Conductance Spectroscopy of Hydrogen-Bonded Complexes. *J. Chem. Phys.* **2017**, *146* (9), 092329.
(29) Mejía, L.; Franco, I. Force−Conductance Spectroscopy of a Single-Molecule Reaction. *Chem. Sci.* **2019**, *10* (11), 3249−3256.
(30) Mejía, L.; Garay-Ruiz, D.; Franco, I. Diels−Alder Reaction in a Molecular Junction. *J. Phys. Chem. C* **2021**, *125* (27), 14599−14606.
(31) Rascón-Ramos, H.; Artés, J. M.; Li, Y.; Hihath, J. Binding Configurations and Intramolecular Strain in Single-Molecule Devices. *Nat. Mater.* **2015**, *14* (5), 517−522.
(32) Ramachandran, R.; Li, H. B.; Lo, W.-Y.; Neshchadin, A.; Yu, L.; Hihath, J. An Electromechanical Approach to Understanding Binding Configurations in Single-Molecule Devices. *Nano Lett.* **2018**, *18* (10), 6638−6644.
(33) (a) Lafferentz, L.; Ample, F.; Yu, H.; Hecht, S.; Joachim, C.; Grill, L. Conductance of a Single Conjugated Polymer as a Continuous Function of Its Length. *Science* **2009**, *323* (5918), 1193−1197. (b) Koch, M.; Ample, F.; Joachim, C.; Grill, L. Voltage-Dependent Conductance of a Single Graphene Nanoribbon. *Nat. Nanotechnol.* **2012**, *7* (11), 713−717. (c) Nacci, C.; Ample, F.; Bleger, D.; Hecht, S.; Joachim, C.; Grill, L. Conductance of a Single Flexible Molecular Wire Composed of Alternating Donor and Acceptor Units. *Nat. Commun.* **2015**, *6* (1), 7397. (d) Kawai, S.; Koch, M.; Gnecco, E.; Sadeghi, A.; Pawlak, R.; Glatzel, T.; Schwarz, J.; Goedecker, S.; Hecht, S.; Baratoff, A.; Grill, L.; Meyer, E. Quantifying the Atomic-Level Mechanics of Single Long Physisorbed Molecular Chains. *Proc. Natl. Acad. Sci. U. S. A.* **2014**, *111* (11), 3968−3972.
(34) Koch, M.; Li, Z.; Nacci, C.; Kumagai, T.; Franco, I.; Grill, L. How Structural Defects Affect the Mechanical and Electrical Properties of Single Molecular Wires. *Phys. Rev. Lett.* **2018**, *121* (4), 047701.

https://doi.org/10.1021/acsomega.1c04785
ACS Omega 2021, 6, 30873−30888